Conducting Boron Sheets Formed by the Reconstruction of the α-Boron (111) Surface

Maximilian Amsler,[1] Silvana Botti,[2] Miguel A. L. Marques,[2] and Stefan Goedecker[1,*]

[1]*Department of Physics, Universität Basel, Klingelbergstrasse 82, 4056 Basel, Switzerland*

[2]*Institut Lumière Matière, UMR5306 Université Lyon 1-CNRS, Université de Lyon, F-69622 Villeurbanne Cedex, France*

(Received 23 May 2013; published 25 September 2013)

Systematic *ab initio* structure prediction was applied for the first time to predict low energy surface reconstructions by employing the minima hopping method on the α-boron (111) surface. Novel reconstruction geometries were identified and carefully characterized in terms of structural and electronic properties. Our calculations predict the formation of a planar, monolayer sheet at the surface, which is responsible for conductive surface states. Furthermore, the isolated boron sheet is shown to be the ground state 2D structure in vacuum at a hole density of $\eta = 1/5$ and is therefore a potential candidate as a precursor for boron nanostructures.

DOI: 10.1103/PhysRevLett.111.136101 PACS numbers: 68.35.bg, 62.23.Kn, 71.15.Mb

Boron exhibits an impressive variety in forming chemical bonds due to its trivalent electronic configuration, ranging from covalent 2-electron 2-center ($2e2c$) bonds to polycentered, metalliclike [1] as well as ionic [2,3] bonding, resulting in a high structural diversity. In the solid state and at ambient conditions, the existence of at least two polymorphs is widely accepted: the low-temperature α-rhombohedral boron phase (α-B) [4] and the high temperature modification of β-rhombohedral boron (β-B) [5,6]. Several other polymorphs have been reported, such as the high-pressure modification γ-B_{28} [2], or the much-disputed tetragonal boron I (t-I) and tetragonal boron II (t-II), also called α-tetragonal [7–9] and β-tetragonal boron [10,11]. The main structural motif of all the above phases is the formation of interlinked B_{12} icosahedra, a common characteristic of many other boron rich compounds which can further contain various different triangular-defined polyhedral building blocks [1].

Recently, immense effort has been made in studying boron structures of lower dimensionality. Theoretical predictions of boron nanotubes [12–14] with metallic conductivity independent of helicity have drawn significant attention in the search for one-dimensional nanostructures. From the experimental point of view there have been reports on mono- and multiwalled boron nanotubes [15,16], boron nanowires [17–21], boron nanorods [22], nanobelts [23], and nanoribbons [24] which may be used for future applications in nanoelectronics. In analogy to carbon nanotubes formed from graphene, boron nanotubes have been theoretically studied by rolling two dimensional boron sheets [25]. In contrast to graphene, boron sheets can be either buckled [26], consisting of a triangular lattice, or, according to more recent predictions, be planar structures with a partially filled honeycomb structure at a specific hole density η, the latter structure being energetically favorable [27,28]. Because of the structural flexibility and the competing energetic ordering, the exact structural and compositional ground state is still under discussion, leading to numerous studies to identify the most stable 2D lattice configuration in vacuum [29–31] and on substrates [32] at different hole densities. Similarly, again inspired by their carbon counterparts, various hollow molecular structures have been theoretically proposed [33–39] in analogy to the C_{60} and other carbon fullerenes [40].

However, there is surprisingly little work on boron at the intermediate dimension between bulk and 2D sheets, namely, on surfaces of boron and boron nanocrystals. Experimental measurements approximate the surface energy of α-B to be in the range of 173–401 meV/Å^2 from cracks in boron fibers [41], and early theoretical studies have been carried out based on empirical potential models resulting in 282 meV/Å^2 for the (111) surface of the same polymorph [42]. *Ab initio* calculations were carried out by Hayami to systematically estimate the energies of low index surfaces in the α-B, β-B, t-I, and t-II phases [43,44]. However, none of the above studies have taken into account any reconstruction mechanisms which are in fact frequently observed in most semiconducting materials. Clearly, reconstructions can lead to considerable decrease in surface energy, thereby significantly altering surface reactivity and other properties.

With increasing computational resources it has become popular to predict structures of crystalline materials and clusters, and, more recently, of 2D planar structures by means of sophisticated global optimization algorithms [45]. The present work, however, goes one step further by applying a structure prediction scheme directly on surfaces to study reconstructions of large boron surfaces with the minima hopping method (MHM) [46,47] based on *ab initio* calculations. Very few studies on *ab initio* predictions of surface reconstructions have been reported in the literature without some sort of input from experiment. The MHM was designed to predict energetically favorable structures by exploring the potential energy surface with a combination of consecutive short molecular dynamic trial steps followed by local geometry optimizations. Many

earlier applications have shown the predictive power of the MHM [48–50], including investigations on surface structures of atomic force microscopy silicon model tips [51,52].

Globally optimizing large surface slabs with more than one hundred atoms is computationally prohibitive when performed at the density functional theory (DFT) level. Therefore, initial MHM simulations were conducted within the density functional based tight binding method, an approximate DFT scheme, as implemented in the DFTB+ package [53], to roughly map out the energy surface and produce a variety of low energy structures, which were subsequently fed back into the MHM using more accurate DFT calculations to refine the search. The projector augmented wave formalism was employed as implemented in VASP [54] using the Perdew-Burke-Erzernhof (PBE) [55] exchange-correlation functional which has been shown to give highly reliable energy differences between different structural motifs in boron [56]. Final results were refined with a plane-wave cutoff energy of 500 eV and sufficiently dense k-point meshes such that the total energy was converged to better than 1 meV per atom. Four additional exchange-correlation functionals were employed to confirm the energetic ordering of the lowest lying structures, namely, PBEsol [57], the local density approximation (LDA), the Heyd-Scuseria-Ernzerhof (HSE06) hybrid functional [58–60], as well as Becke-Lee-Yang-Parr (BLYP) [61,62] within the ABINIT plane wave DFT code [63,64]. Geometries were fully relaxed with a tight convergence criteria of less than 0.004 eV/Å for the maximal force components.

α-B is described by cubic close packing of B_{12} units, while planes of icosahedra are stacked in ABC order along the $\langle 111 \rangle$ direction [see Figs. 1(a) and 1(b) where the bulk layers are depicted by orange icosahedra]. The MHM simulations were conducted on slabs with up to 4 layers of B_{12} units while at least all atoms in the topmost icosahedral layer were allowed to move during the search. The majority of our simulations were performed on a supercell $\{\mathbf{a}_S, \mathbf{b}_S, \mathbf{c}_S\}$ generated from the rhombohedral cell vectors $\{\mathbf{a}_R, \mathbf{b}_R, \mathbf{c}_R\}$, containing ≈ 100 atoms and such that a surface area of 62.6 Å^2 was covered: $\mathbf{a}_S = 2\mathbf{a}_R - \mathbf{b}_R - \mathbf{c}_R$, $\mathbf{b}_S = \mathbf{a}_R + \mathbf{b}_R - 2\mathbf{c}_R$ and $\mathbf{c}_S = \alpha(\mathbf{a}_R + \mathbf{b}_R + \mathbf{c}_R)$, for $\alpha > 1$. To prevent interactions with periodic images along the surface-normal direction, initial searches were conducted with a vacuum layer of ≈ 6 Å. The final results were obtained with a vacuum space of more than 7 Å, a value at which the surface energy was converged better than 1 meV/Å^2. Surface energies were computed according to $\sigma = (1/2A)(N\epsilon_{\text{bulk}} - E_{\text{slab}})$, where A denotes the surface area, ϵ_{bulk} is the energy per atom in the crystalline phase (here α-B) and E_{slab} is the energy of the slab containing N atoms.

Earlier investigations by Hayami *et al.* [44] on unreconstructed (111) surfaces indicated a difference in surface energy depending on whether the surface was formed by inter- or intraicosahedral cuts. According to their results obtained with BLYP, a surface obtained by cutting between icosahedral planes, denoted as (111)-I, would destroy the presumably strong intericosahedral bonds and thus lead to a higher surface energy compared to performing a cut through the weaker intraicosahedral bonds, denoted as (111)-II. However, when reconstructions are permitted, this simple characterization based on bond breaking can easily fail. In fact, the number of mobile surface atoms is much more important since it can lead to unexpected structural rearrangements and the formation of new, energetically favorable bonds. Therefore, MHM simulations were performed on both the (111)-I and (111)-II surfaces and the results were summarized in Table I. Strikingly, the

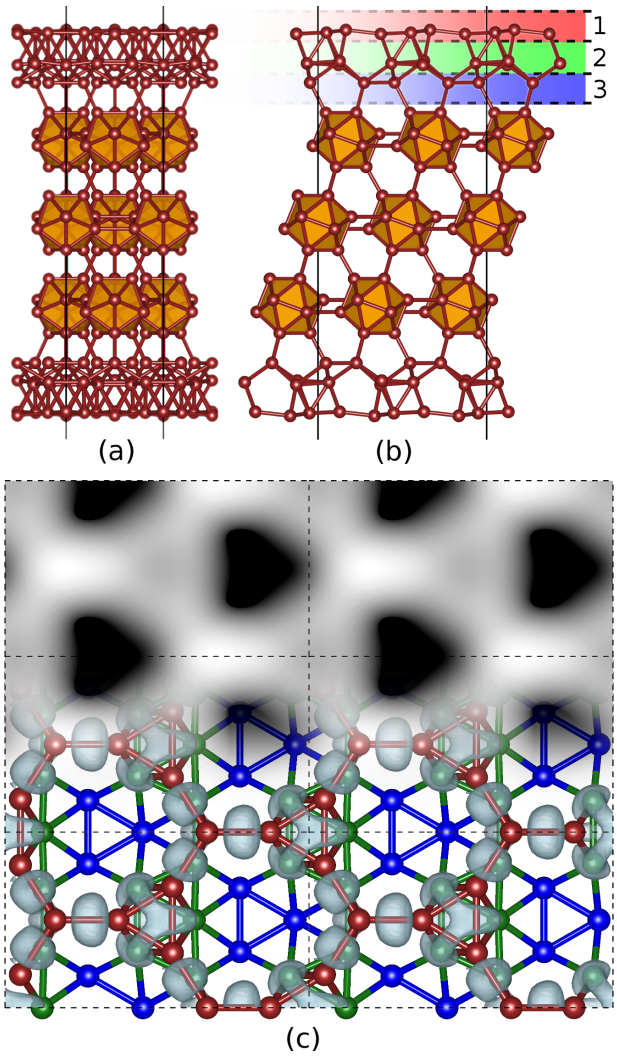

FIG. 1 (color online). View from the $\langle 11\bar{2} \rangle$ (a) and the $\langle 1\bar{1}0 \rangle$ (b) direction of (111)-$I_{R,(h)}$. (c) Top view toward the surface from the $\langle \bar{1}\,\bar{1}\,\bar{1} \rangle$ direction. The colors red (light gray), green (medium gray), and blue (dark gray) denote the first, second, and third atomic layer, respectively. An isosurface of the ELF is shown for the top two layers at the bottom, and the STM image is overlayed at the top.

TABLE I. Lowest energy surfaces, sorted with respect to surface types. The surface energies are given for different functionals where available in units of meV/Å^2 (NA stands for not available). The lowest reconstructed structures (111)-I/II$_{R,(\alpha)}$ are given in the second section, enumerated $\alpha = a, b, \ldots$ according to the PBE energetic ordering. Energy differences are given with respect to (111)-I/II$_{R,(a)}$. Reconstructed surfaces with three additional and three missing atoms per supercell are denoted as (111)-I$_R^+$ and (111)-I$_R^-$, respectively.

Surface	PBE	PBEsol	LDA	HSE[a]	BLYP
Nonreconstructed					
(111)-I	218.8	233.3	236.5	247.5	205.4 220.0[b]
(111)-II	215.6	227.2	231.7	250.2	167.1 170.0[b]
Reconstructed (111)-I					
(111)-I$_{R,(a)}$	170.61	181.57	190.39	196.31	NA
(111)-I$_{R,(b)}$	+1.54	+1.32	+1.94	+2.28	NA
(111)-I$_{R,(c)}$	+1.85	+1.77	+1.99	+1.70	NA
(111)-I$_{R,(d)}$	+2.46	+2.57	+2.30	+2.08	NA
(111)-I$_{R,(e)}$	+2.98	+3.06	+2.36	+2.05	NA
(111)-I$_{R,(f)}$	+3.20	+3.40	+2.85	+3.45	NA
(111)-I$_{R,(g)}$	+3.21	+3.27	+2.94	+2.89	NA
(111)-I$_{R,(h)}$	+3.71	+4.02	+2.12	+2.42	NA
(111)-I$_{R,(i)}$	+4.76	+4.79	+4.39	+3.44	NA
Reconstructed (111)-II					
(111)-II$_{R,(a)}$	183.0	200.8	206.6	210.0	NA
Reconstructed (111)-I, atoms added					
(111)-I$^+_{R,(a)}$	199.4	212.4	217.9	226.1	NA
Reconstructed (111)-I, atoms removed					
(111)-I$^-_{R,(a)}$	180.4	194.6	201.3	204.6	NA

[a]Structure relaxed with PBE.
[b]Taken from Ref. [44].

energetic difference of the unreconstructed (111)-I and (111)-II surfaces depend strongly on the employed exchange-correlation functional (first section in Table I). While PBE, PBEsol, LDA, and HSE06 are in good agreement and predict a small energy difference of 3–5 meV/Å^2 between (111)-I and (111)-II, BLYP gives a higher value of 40–50 meV/Å^2, suggesting that the difference between inter- and intraicosahedral bond energies is less prominent than assumed by Hayami *et al.* [44]. The lowest energies of the reconstructed surfaces (111)-I$_{R,(a)}$ and (111)-II$_{R,(a)}$ from the MHM simulations are also summarized in Table I and clearly show that (111)-I$_{R,(a)}$ is energetically favored, in contrast to the unreconstructed counterparts.

The arrangement of the atoms in the structure (111)-I$_{R,(h)}$ is shown in Fig. 1, where panel (a) and (b) represent the side views along the $\langle 11\bar{2}\rangle$ and the $\langle 1\bar{1}0\rangle$ direction, respectively. The three outer atomic layers participate in the reconstruction and are shown separately in panel (c). The first atomic layer, colored in red (light gray), forms an almost planar filament of interlinked triangular pattern with *Cmmm* symmetry. It is identical for all low energy structures that were found during the MHM simulations, thus providing the fundamental structure to terminate the surface. This first layer is supported by a second atomic layer of higher complexity comprised by a denser network of triangular units (green or medium gray), thereby forming octahedra together with the triangles from the first layer. The structural variety in this layer, however, is much larger as illustrated in Fig. 2. The corresponding energies are given in the second section of Table I which show that the energetic differences resulting from the subtle rearrangements of the triangles are very small, preventing an unambiguous identification of the ground state structure. Finally, the third layer is again identical for all low-energy structures (shown in blue or dark gray) and these are simply the remaining base planes of the underlying icosahedral bulk structure.

In contrast to (111)-I$_R$, the reconstructed (111)-II$_R$ surfaces do not form any planar structures. Since only half of the atoms are available for reconstruction due to the intraicosahedral truncation, the number of mobile surface atoms is insufficient to satisfy an energetically optimal bonding configuration. Although an additional layer of icosahedra was explicitly included to rearrange during the MHM simulation, the atoms in this layer did not participate in the reconstruction and retained the bulk arrangement. The basic structural motif for all low-energy (111)-II$_R$ surfaces essentially consists of loosely connected nanoribbons with a triangular pattern on top of a perfect icosahedra layer of the bulk slab.

The compositional stability of the surface reconstructions was further investigated by adding and subtracting atoms to the surface layers and performing further MHM simulations (the last two sections of Table I). When

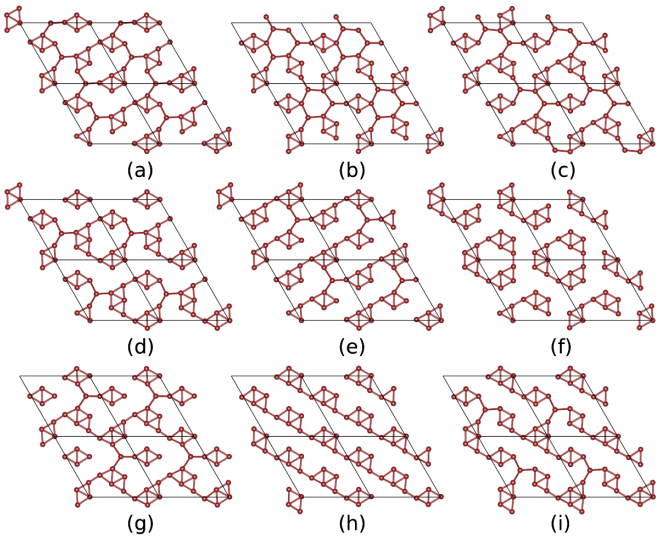

FIG. 2 (color online). The second atomic layer of the nine lowest energy surface structures (111)-I$_{R,(\alpha)}$, $\alpha = a, b, \ldots$, are shown.

depositing atoms (up to 3 atoms per supercell) on the reconstructed surface no structural changes were observed both in the second and third atomic surface layers. The additional atoms clustered on the top layer by forming trigonal structures oriented away from the surface. The surface energy of the lowest structure of this type, (111)-$I^{+}_{R,(a)}$, was found to be 28.74 meV/Å^2 higher in energy than the lowest reconstructed structure (111)-$I_{R,(a)}$. Similarly, removing atoms from the surface layer (up to 3 atoms per supercell) resulted in the reordering of the topmost layer without significantly disturbing the second and third atomic layers. In fact, in the case of removing 3 atoms per supercell, the top layer was reconstructed such that a triangular unit was missing, thus destroying an octahedron initially formed together with the second layer. Although still endothermic, the energy difference of (111)-$I^{-}_{R,(a)}$ with respect to the clean slab (111)-$I_{R,(a)}$ is smaller with a value of 9.75 meV/Å^2. It can therefore be concluded that the stoichiometry obtained by a planar cut through the bulk is indeed the most stable.

Finally, the electronic structure was studied by investigating the electron localization function (ELF) [65] as implemented in VASP. Figure 1(c) shows a corresponding ELF isosurface of the two top atomic surface layers. A clear distinction can be made between the $2e2c$ bonds in the topmost layer connecting the triangular units in the plane, and the polycentric bonds which dominate within all triangular arrangements, especially in the octahedra formed between the first and the second layer. This mixture of covalent $2e2c$ and the polycentric bonding system is characteristic also in the bulk region, where the intraicosahedral bonds are purely polycentric and intericosahedral bonds are either two-centered (between planes) or three-centered (within the plane). Additionally, a constant current scanning tunnel microscopy (STM) simulation was performed at a bias of $V_b = -1.5$ eV based on the Tersoff-Hamann approximation [66]. The constant current image at a maximal height of ≈ 1.8 Å above the surface was rendered on top of Fig. 1(c) which can be qualitatively compared to STM experiments .

Furthermore, the electronic surface band structure was calculated within the 2D-Brillouin zone for both the reconstructed and the nonreconstructed surface as shown in Fig. 3. The projected band structure of bulk α-B, shown as the shaded region in orange, has a PBE band gap with a value of 1.47 eV. When a vacuum is introduced into the material without further reconstruction, the conduction bands decrease and appear as surface states in the gap region, which reduce its magnitude to 0.50 eV (shown as dashed green lines). However, conducting surface states emerge upon allowing the surface to reconstruct, crossing the Fermi level and thus forming a metallic surface (shown as solid red lines). Since conventional DFT commonly underestimates the band gap, additional calculations were performed with the HSE06 hybrid functional, leading to a

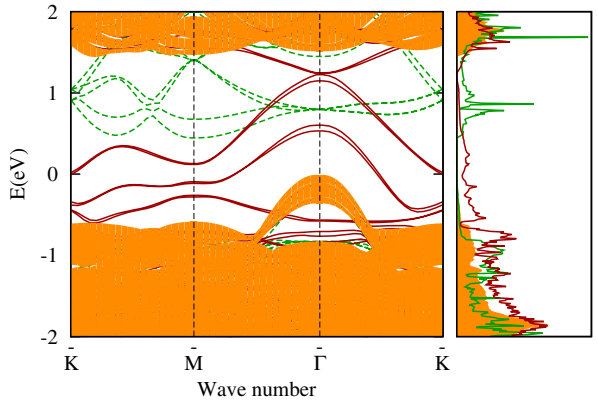

FIG. 3 (color online). The electronic surface band structures and the density of states of the (111)-I surface are shown. Orange lines (shaded) indicate bulk bands, whereas the red (solid) lines represent the surface states of the reconstructed surface. The green (dashed) lines represent the surface bands of the unreconstructed surface of α-B. The energy zero is set at the Fermi energy of the bulk.

bulk gap of 2.02 and 0.86 eV for the unreconstructed (111)-I. Earlier theoretical works have predicted many 2D boron sheets to be metallic as well [29–31] such that one way of interpreting the above results is as if a planar, conducting sheet of boron is adsorbed on a (111) α-B surface. Based on this perception the stability of the topmost atomic layer was investigated when isolated from the surface. A simple local geometry relaxation was performed in vacuum while allowing the cell to adjust according to the in-plane stresses, starting from the initial structure shown in Fig. 4(a). As expected, this structure is metallic and transformed to a more compact state upon relaxation to compensate the missing interaction with the substrate. The final structure is shown in Fig. 4(c), which has previously been predicted to be the ground state in boron sheets at a

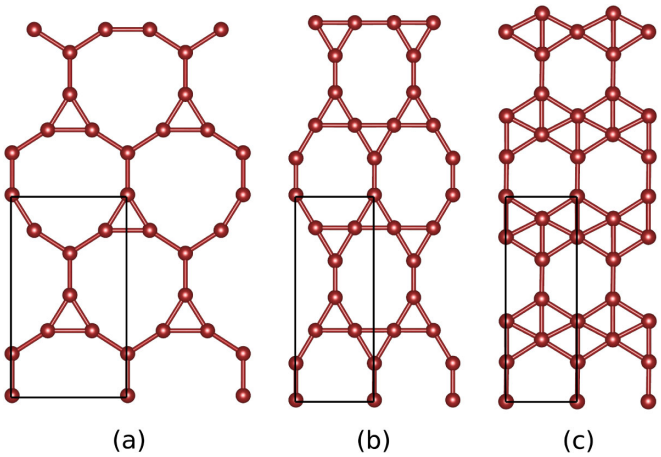

FIG. 4 (color online). Structural transformation of the topmost atomic layer of the reconstructed surface during a local geometry optimization. (a) Initial structure, (b) intermediate during relaxation, and (c) final structure, relaxed into the global minimum of 2D sheets at $\eta = 1/5$ hole density.

fixed hole density of $\eta = 1/5$, denoted as "struc-1/5" in Ref. [29]. No imaginary phonon frequencies were found in the whole 2D-Brillouin zone, indicating that the 2D structure is dynamically stable. The energy difference between (111)-$I_{R,(a)}$ and the isolated sheet plus the optimized, remaining slab is merely 54.4 meV/Å^2, a value comparable with the exfoliation energy of graphene (20.0 meV/Å^2) [67]. This sheet configuration is again metallic and could provide a promising precursor for other boron nanostructures such as single-walled boron nanotubes or cage molecules.

In conclusion, an extensive, systematic *ab initio* structural search was for the first time performed with the MHM on surfaces to identify reconstruction geometries. The main structural motif of the reconstructed (111) surface of α-B was isolated, studied, and accurately characterized. In contrast to the unreconstructed surface (111)-I, which merely reduces the band gap of crystalline α-B, the reconstructed (111)-I_R structures contains metallic surface states that facilitates electric conduction. The topmost layers of all low energy reconstructions (111)-I_R are planar and consist of a 2D network of interlinked triangular patterns. These results can be interpreted as if a conducting sheet of boron was adsorbed on a semiconducting substrate, leading to numerous possible applications in nanoelectronics. Assuming that it is further possible to isolate the top monolayer of boron through exfoliation it would provide a 2D boron sheet with $\eta = 1/5$ hole density as a promising precursor for a large variety of boron nanostructures. The present results will certainly stimulate future experimental and theoretical studies on boron surfaces and boron nanostructures.

Financial support provided by the Swiss National Science Foundation and French ANR (ANR-08-CEXC8-008-01 and ANR-12-BS04-0001-02) are gratefully acknowledged. Computational resources were provided by the Swiss National Supercomputing Center (CSCS) in Lugano and French GENCI (Project No. x2013096017).

*Stefan.Goedecker@unibas.ch

[1] B. Albert and H. Hillebrecht, Angew. Chem., Int. Ed. **48**, 8640 (2009).
[2] A. R. Oganov, J. Chen, C. Gatti, Y. Ma, Y. Ma, C. W. Glass, Z. Liu, T. Yu, O. O. Kurakevych, and V. L. Solozhenko, Nature (London) **457**, 863 (2009).
[3] S. Mondal, S. van Smaalen, A. Schönleber, Y. Filinchuk, D. Chernyshov, S. I. Simak, A. S. Mikhaylushkin, I. A. Abrikosov, E. Zarechnaya, L. Dubrovinsky, and N. Dubrovinskaia, Phys. Rev. Lett. **106**, 215502 (2011).
[4] L. V. McCarty, J. S. Kasper, F. H. Horn, B. F. Decker, and A. E. Newkirk, J. Am. Chem. Soc. **80**, 2592 (1958).
[5] D. E. Sands and J. L. Hoard, J. Am. Chem. Soc. **79**, 5582 (1957).
[6] R. E. Hughes, C. H. L. Kennard, D. B. Sullenger, H. A. Weakliem, D. E. Sands, and J. L. Hoard, J. Am. Chem. Soc. **85**, 361 (1963).
[7] A. W. Laubengayer, D. T. Hurd, A. E. Newkirk, and J. L. Hoard, J. Am. Chem. Soc. **65**, 1924 (1943).
[8] J. L. Hoard, J. Am. Chem. Soc. **73**, 1892 (1951).
[9] J. L. Hoard, R. E. Hughes, and D. E. Sands, J. Am. Chem. Soc. **80**, 4507 (1958).
[10] C. P. Talley, S. La Placa, and B. Post, Acta Crystallogr. **13**, 271 (1960).
[11] M. Vlasse, R. Naslain, J. Kasper, and K. Ploog, J. Less Common Metals **67**, 1 (1979).
[12] I. Boustani and A. Quandt, Europhys. Lett. **39**, 527 (1997).
[13] A. Gindulyt, W. N. Lipscomb, and L. Massa, Inorg. Chem. **37**, 6544 (1998).
[14] I. Boustani, A. Quandt, E. Hernndez, and A. Rubio, J. Chem. Phys. **110**, 3176 (1999).
[15] D. Ciuparu, R. F. Klie, Y. Zhu, and L. Pfefferle, J. Phys. Chem. B **108**, 3967 (2004).
[16] F. Liu, C. Shen, Z. Su, X. Ding, S. Deng, J. Chen, N. Xu, and H. Gao, J. Mater. Chem. **20**, 2197 (2010).
[17] L. M. Cao, Z. Zhang, L. L. Sun, C. X. Gao, M. He, Y. Q. Wang, Y. C. Li, X. Y. Zhang, G. Li, J. Zhang, and W. K. Wang, Adv. Mater. **13**, 1701 (2001).
[18] C. J. Otten, O. R. Lourie, M.-F. Yu, J. M. Cowley, M. J. Dyer, R. S. Ruoff, and W. E. Buhro, J. Am. Chem. Soc. **124**, 4564 (2002).
[19] J. Tian, J. Cai, C. Hui, C. Zhang, L. Bao, M. Gao, C. Shen, and H. Gao, Appl. Phys. Lett. **93**, 122105 (2008).
[20] F. Liu, J. Tian, L. Bao, T. Yang, C. Shen, X. Lai, Z. Xiao, W. Xie, S. Deng, J. Chen, J. She, N. Xu, and H. Gao, Adv. Mater. **20**, 2609 (2008).
[21] J. Tian, C. Hui, L. Bao, C. Li, Y. Tian, H. Ding, C. Shen, and H.-j. Gao, Appl. Phys. Lett. **94**, 083101 (2009).
[22] D. Zhu and E. Kisi, J. Australian Ceram. Soc. **45**, 49 (2009).
[23] Z. Wang, Y. Shimizu, T. Sasaki, K. Kawaguchi, K. Kimura, and N. Koshizaki, Chem. Phys. Lett. **368**, 663 (2003).
[24] T. T. Xu, J.-G. Zheng, N. Wu, A. W. Nicholls, J. R. Roth, D. A. Dikin, and R. S. Ruoff, Nano Lett. **4**, 963 (2004).
[25] A. Quandt and I. Boustani, ChemPhysChem **6**, 2001 (2005).
[26] J. Kunstmann, A. Quandt, and I. Boustani, Nanotechnology **18**, 155703 (2007).
[27] H. Tang and S. Ismail-Beigi, Phys. Rev. Lett. **99**, 115501 (2007).
[28] H. Tang and S. Ismail-Beigi, Phys. Rev. B **82**, 115412 (2010).
[29] X. Yu, L. Li, X.-W. Xu, and C.-C. Tang, J. Phys. Chem. C **116**, 20 075 (2012).
[30] X. Wu, J. Dai, Y. Zhao, Z. Zhuo, J. Yang, and X. C. Zeng, ACS Nano **6**, 7443 (2012).
[31] H. Lu, Y. Mu, H. Bai, Q. Chen, and S.-D. Li, J. Chem. Phys. **138**, 024701 (2013).
[32] Y. Liu, E. S. Penev, and B. I. Yakobson, Angew. Chem., Int. Ed. **52**, 3156 (2013).
[33] M. A. L. Marques and S. Botti, J. Chem. Phys. **123**, 014310 (2005).
[34] N. Gonzalez Szwacki, A. Sadrzadeh, and B. I. Yakobson, Phys. Rev. Lett. **98**, 166804 (2007).

[35] S. Botti, A. Castro, N. N. Lathiotakis, X. Andrade, and M. A. L. Marques, Phys. Chem. Chem. Phys. **11**, 4523 (2009).
[36] C. Ozdogan, S. Mukhopadhyay, W. Hayami, Z. B. Guvenc, R. Pandey, and I. Boustani, J. Phys. Chem. C **114**, 4362 (2010).
[37] K. D. Quarles, C. B. Kah, R. N. Gunasinghe, R. N. Musin, and X.-Q. Wang, J. Chem. Theory Comput. **7**, 2017 (2011).
[38] P. Pochet, L. Genovese, S. De, S. Goedecker, D. Caliste, S. A. Ghasemi, K. Bao, and T. Deutsch, Phys. Rev. B **83**, 081403 (2011).
[39] F. Li, P. Jin, D.-e. Jiang, L. Wang, S. B. Zhang, J. Zhao, and Z. Chen, J. Chem. Phys. **136**, 074302 (2012).
[40] H. W. Kroto, J. R. Heath, S. C. O'Brien, R. F. Curl, and R. E. Smalley, Nature (London) **318**, 162 (1985).
[41] J. Vega-Boggio, J.-Å. Schweitz, and O. Vingsbo, J. Mater. Sci. **12**, 1692 (1977).
[42] J. Vega-Boggio and J.-Å. Schweitz, J. Mater. Sci. **12**, 1923 (1977).
[43] W. Hayami and S. Otani, J. Phys. Chem. C **111**, 10 394 (2007).
[44] W. Hayami and S. Otani, J. Phys. Chem. C **111**, 688 (2007).
[45] A. R. Oganov, *Modern Methods of Crystal Structure Prediction* (Wiley-VCH, New York, 2010).
[46] S. Goedecker, J. Chem. Phys. **120**, 9911 (2004).
[47] M. Amsler and S. Goedecker, J. Chem. Phys. **133**, 224104 (2010).
[48] M. Amsler, J. A. Flores-Livas, L. Lehtovaara, F. Balima, S. A. Ghasemi, D. Machon, S. Pailhès, A. Willand, D. Caliste, S. Botti, A. San Miguel, S. Goedecker, and M. A. L. Marques, Phys. Rev. Lett. **108**, 065501 (2012).
[49] J. A. Flores-Livas, M. Amsler, T. J. Lenosky, L. Lehtovaara, S. Botti, M. A. L. Marques, and S. Goedecker, Phys. Rev. Lett. **108**, 117004 (2012).
[50] M. Amsler, J. A. Flores-Livas, T. D. Huan, S. Botti, M. A. L. Marques, and S. Goedecker, Phys. Rev. Lett. **108**, 205505 (2012).
[51] S. A. Ghasemi, S. Goedecker, A. Baratoff, T. Lenosky, E. Meyer, and H. J. Hug, Phys. Rev. Lett. **100**, 236106 (2008).
[52] M. Amsler, S. A. Ghasemi, S. Goedecker, A. Neelov, and L. Genovese, Nanotechnology **20**, 445301 (2009).
[53] B. Aradi, B. Hourahine, and T. Frauenheim, J. Phys. Chem. A **111**, 5678 (2007).
[54] G. Kresse and J. Furthmüller, Comput. Mater. Sci. **6**, 15 (1996); G. Kresse and J. Hafner, Phys. Rev. B **47**, 558 (1993); G. Kresse and J. Furthmüller, Phys. Rev. B **54**, 11 169 (1996); G. Kresse and D. Joubert, Phys. Rev. B **59**, 1758 (1999).
[55] J. P. Perdew, K. Burke, and M. Ernzerhof, Phys. Rev. Lett. **77**, 3865 (1996).
[56] C. R. Hsing, C. M. Wei, N. D. Drummond, and R. J. Needs, Phys. Rev. B **79**, 245401 (2009).
[57] J. P. Perdew, A. Ruzsinszky, G. I. Csonka, O. A. Vydrov, G. E. Scuseria, L. A. Constantin, X. Zhou, and K. Burke, Phys. Rev. Lett. **100**, 136406 (2008).
[58] J. Heyd, G. E. Scuseria, and M. Ernzerhof, J. Chem. Phys. **118**, 8207 (2003).
[59] J. Paier, M. Marsman, K. Hummer, G. Kresse, I. C. Gerber, and J. G. Ángyán, J. Chem. Phys. **125**, 249901 (2006).
[60] J. Heyd, G. E. Scuseria, and M. Ernzerhof, J. Chem. Phys. **124**, 219906 (2006).
[61] A. D. Becke, Phys. Rev. A **38**, 3098 (1988).
[62] C. Lee, W. Yang, and R. G. Parr, Phys. Rev. B **37**, 785 (1988).
[63] X. Gonze, G.-M. Rignanese, M. Verstraete, J.-M. Beuken, Y. Pouillon, R. Caracas, F. Jollet, M. Torrent, G. Zerah, M. Mikami, P. Ghosez, M. Veithen, J.-Y. Raty, V. Olevano, F. Bruneval, L. Reining, R. Godby, G. Onida, D. Hamann, and D. Allan, Z. Kristallogr. **220**, 558 (2005).
[64] F. Bottin, S. Leroux, A. Knyazev, and G. Zrah, Comput. Mater. Sci. **42**, 329 (2008).
[65] B. Silvi and A. Savin, Nature (London) **371**, 683 (1994).
[66] J. Tersoff and D. R. Hamann, Phys. Rev. B **31**, 805 (1985).
[67] T. Gould, S. Lebgue, and J. F. Dobson, arXiv:1306.1673.